Draft version February 1, 2008
Preprint typeset using LaTeX style emulateapj v. 04/03/99

THE MEASUREMENT OF DISK ELLIPTICITY IN NEARBY SPIRAL GALAXIES

David R. Andersen
Department of Astronomy and Astrophysics, Pennsylvania State University, 525 Davey Lab, University Park, PA 16802; andersen@astro.psu.edu.
Matthew A. Bershady, Linda S. Sparke, John S. Gallagher, III, Eric M. Wilcots
Department of Astronomy, University of Wisconsin, 475 N Charter Street, Madison, WI 53706; mab@astro.wisc.edu, sparke@astro.wisc.edu, jsg@astro.wisc.edu, ewilcots@astro.wisc.edu.

Draft version February 1, 2008

ABSTRACT

We have measured the intrinsic disk ellipticity for 7 nearby, nearly face–on spiral galaxies by combining Densepak integral-field spectroscopy with I-band imaging from the WIYN telescope. Initially assuming an axisymmetric model, we determine kinematic inclinations and position angles from Hα velocity fields, and photometric axis ratios and position angles from imaging data. We interpret the observed disparities between kinematic and photometric disk parameters in terms of an intrinsic non-zero ellipticity, ϵ. The mean ellipticity of our sample is 0.05. If the majority of disk galaxies have such intrinsic axis ratios, this would account for roughly 50% of the scatter in the Tully–Fisher relation. This result, in turn, places tighter constraints on other sources of scatter in this relation, the most astrophysically compelling of which is galaxy mass-to-light ratios.

Subject headings: galaxies: structure – galaxies: kinematics

1. INTRODUCTION

A large fraction of galaxy disks appears to be non-axisymmetric. Photometric studies of face–on galaxies find the light distribution in 30–50% of spirals is lopsided ($m = 1$ distortions; Zaritsky & Rix, 1997; Rudnick & Rix, 1998) or has higher order distortions ($m \geq 2$; Rix & Zaritsky, 1995; Kornreich et al., 1998; Conselice et al., 2000). A similar fraction of galaxies has lopsided HI distributions or kinematic asymmetries (Baldwin et al., 1980; Bosma, 1981; Richter & Sancisi, 1994; Haynes et al., 1998; Swaters et al., 1999).

Disk ellipticity ($m = 2$) may also be common. Few disk galaxies appear round on the sky; the distribution of apparent axis ratios is best modeled by randomly oriented disks with intrinsic ellipticities $\epsilon \sim 0.1$ (Binney & de Vaucouleurs, 1981; Grøsbol, 1985; Huizinga & van Albada, 1992; Lambas et al., 1992). These statistical studies constrain mean ellipticity, but do not probe the intrinsic ellipticity of individual galaxies.

If galaxy disks are elongated, errors in photometric estimates of inclinations and position angles (PAs) will be introduced, thereby contributing to the scatter in the relationship between galaxy luminosity and rotation speed (Tully & Fisher, 1977). Franx & de Zeeuw (1992) used a specific, non-rotating velocity field model to show that if $\epsilon = 0.1$ on average, systematic errors could account for all the observed scatter in the Tully–Fisher (hereafter, TF) relation. However, the true contribution to this scatter depends on the distribution of intrinsic axis ratios. Identifying the individual ellipticities of galaxies would limit other sources of astrophysical scatter in the TF relation and reduce scatter.

Kinematic maps can be used to estimate ellipticity for individual galaxy disks. One approach involves fitting such maps with elliptic orbits, from which a quantity related to the ellipticity of the potential can be estimated: $\epsilon_{\rm pot} \sin 2\phi$. This quantity varies from 0.001 – 0.07 for a sample of 9 galaxies (Schoenmakers et al., 1997; Schoenmakers, 1999). Unfortunately, the phase angle ϕ is not directly measurable. Such studies have been rare because they require observationally expensive, high resolution, high signal-to-noise velocity field maps (e.g. Teuben et al., 1986; Kornreich et al., 2000).

Here we develop a new, efficient method of estimating intrinsic galaxy disk ellipticities using optical kinematic maps and photometric indices. Determining unique solutions for ϵ and ϕ requires measurements of both kinematic and photometric inclination and PAs for nearly face–on spiral disks. When the disk major axis is rotated by a phase angle ϕ away from the line of nodes, the kinematic and photometric axes will appear misaligned only if $\cos i < 1 - \epsilon$. If $\epsilon \approx 0.1$, as suggested by earlier studies, substantial misalignment of kinematic and photometric PAs ($> 30°$) will occur only for galaxies with $i < 30°$. To demonstrate our method we present the detailed analysis of WIYN integral field Hα velocity fields and I band images for UGC 4380, and measurements of ϵ for an additional 6, nearly face–on galaxies based on the same method.

2. SAMPLE AND OBSERVATIONS

Our sample of seven galaxies is a subset of 69 selected from the *Principal Galaxy Catalog* (PGC; Paturel et al., 1997) in regions of low Galactic extinction with normal surface-brightnesses, axis ratios corresponding to $< 30°$ inclination for a circular disk, diameters D_{25} between 0.75 and 1.5 arcminutes (to facilitate spectroscopic follow-up), and Hubble types between Sb and Sc (see Andersen et al., 2001). We excluded galaxies with obvious bars, clearly visible non-axisymmetric structure, and foreground stars within 2-4 disk scale lengths using the Second Palomar Observatory Sky Survey.

We used the WIYN S2KB imager (a 2048^2 CCD with 0.195 arcsec/pixel) to obtain deep I-band images of our

7 targets between May 10-14, 1999 with seeing of $\sim$1.1 arcseconds FWHM, or 10% of 1 scale length. We reduced these images using standard procedures, yielding sufficient signal-to-noise to establish galaxy isophotes to ~ 4.5 scale lengths. We used flux-calibrated, R-band magnitudes obtained with the IGI/TK4 imager on the McDonald Observatory 107" telescope to check that these galaxies had close to "Freeman" disks (B-band central disk surface brightness of 21.7 mag arcsec^{-2}). For example, assuming $B - R = 1.15$ for the Sc-type galaxy UGC 4380, we find $\mu_0(B) = 21.5$ mag arcsec^{-2}.

Spectral images of our 7 targets were obtained using Densepak on the WIYN telescope from portions of runs on May 20-21, 1998, January 20-22, 1999, and March 27-28, 1999. Densepak is a fiber-optic array used for integral field spectroscopy containing 86 active, 3-arcsecond fibers (separated by 4 arcseconds) arranged in a 7×13 staggered grid subtending an area of 30×45 arcseconds (Barden et al., 1998). Four additional "sky" fibers are spaced around this grid roughly one arcminute from the grid center. Densepak feeds the WIYN Bench Spectrograph, which we used with an echelle grating to cover $6600\text{Å} < \lambda\lambda < 7000\text{Å}$ with a dispersion of 0.19 Å per pixel and a FWHM spectral resolution of 0.51 Å. Basic spectral reductions were done using the NOAO *IRAF* package *dohydra*. Thorium-Argon lamps were used for wavelength calibration.

Since galaxy rotation curves peak at roughly two photometric scale lengths (Courteau & Rix, 1999; Willick, 1999), we used Densepak to map out to ~ 3 scale lengths per galaxy (typically ~ 30 arcsec). For UGC 4380, which has a I-band scale length of 9.7 arcseconds, two Densepak pointings were required to cover a square of roughly 45×45 square arcseconds. Two 30-minute exposures were made at each Densepak position to facilitate cosmic ray removal. The Hα line flux was typically measured at a signal to noise of ~ 10 at the edge of our observed field.

3. MEASUREMENTS

To measure photometric axis ratios and PAs we use the STSDAS ISOPHOTE package *ellipse* on images with stars masked. Figure 1 shows the radial dependence of PA, apparent ellipticity (1-b/a), and an azimuthal variance statistic for UGC 4380. Inside 29 arcseconds, the variance statistic is greater than unity showing that spiral arm structure affects the ellipse fits. Hence we measure the photometric axis ratio and PA at radii greater than 29 arcseconds, where the axis ratio and PA are constant, consistent with our estimate that spiral structure has a minimal impact.

To determine kinematic inclination and PAs, we first produce Hα emission line maps from the 86 field-flattened and sky-subtracted spectra from each pointing. We measure velocity centroids by fitting a Gaussian line profile to each Hα line, and assign a spatial position based on the fiber geometry of Densepak and the offsets used to make multiple pointings. Figure 2 shows a polynomial surface fit to these discrete velocity measurements for UGC 4380. UGC 4380 clearly is an inclined galaxy with a center coincident with the photometric center. The formally well-determined PA and peak rotation velocity (Table 1) agree with visual inspection of the data (Figure 2). Single dish HI observations of UGC 4380 list a W_{50} velocity widths of 118 km/s (Haynes et al., 1988). The W_{50} width measured from our Densepak spectra is also 118 km/s, implying we observed the peak of the rotation curve.

To extract the PA, peak velocity and inclination, we fit the velocities expected at each fiber position using a simple model consisting of concentric and coplanar circular orbits with $V(r) = V_c \tanh(r/h)$, where the terminal circular velocity V_c and h are free parameters. The other free variables are inclination, PA, center, and central velocity. Our velocity fields exhibit only small deviations from this simple model, as illustrated for UGC 4380 in the middle panel of Figure 2. The best fitting model was determined from χ^2 minimization (downhill simplex method) based on comparing the measured velocity centroids, fiber by fiber with the smooth model velocity field sampled with the Densepak footprint. The standard deviation in the fit residuals is 4.3 km/s. More elaborate radial velocity functions do not provide smaller residuals yet have more independent variables. Formal confidence limits (CL) were placed on these quantities by determining surfaces of constant χ^2. Table 1 contains our measurements of axis ratio, photometric PA and kinematic inclination and PA. In UGC 4380, the photometric and kinematic PA differ by $9.5^\circ \pm 3.9^\circ$ (68% CL). This disk is unlikely to be intrinsically circular.

4. ANALYSIS AND RESULTS

We can estimate the ellipticity required to produce the above level of discrepancy by modeling the observed galaxy as a disk with intrinsic, photometric ellipticity ϵ (right panel, Figure 2) but circular orbits (justified below). The vector describing the ellipse in the galaxy plane is $\vec{r}\,' = [-(1-\epsilon)\sin\theta, \cos\theta]$, where $\theta = 0$ is the major axis. To project the ellipse onto the (observed) sky plane, it is inclined by an angle i about the line of nodes at an angle ϕ from the intrinsic major axis. In the plane of the sky, the ellipse describing the galaxy isophotes is given by a transformation matrix involving θ, i, ϵ, and ϕ.

Franx & de Zeeuw (1992) found that for orbits in a flat but elliptic disk, fitting the velocity field with tilted circular rings yields the correct disk orientation to first order in ellipticity. Accordingly, we take the kinematic inclination and PAs to represent the true inclination and PA of the disk; ϵ and ϕ can then be determined given measurements of the apparent photometric axis ratio (b/a), the kinematic inclination (i), and the difference between photometric and kinematic PAs (ψ).

When the true inclination i is closer to face–on than the photometric inclination, as is the case for UGC 4380, the galaxy must be at least as flattened as $\epsilon \geq 1 - \frac{b}{a}\cos i^{-1}$. The intrinsic flattening must be even larger if the true major axis does not lie in the plane of the sky. This lower limit for UGC 4380, $\epsilon > 0.06 \pm 0.03$, is inconsistent with a purely circular disk. By utilizing the $9.5^\circ \pm 3.9^\circ$ misalignment of the photometric and kinematic PAs, a better estimate of the ellipticity can be obtained.

In general, three equations relate the three observables b/a, i, and ψ to the three unknowns ϵ, ϕ, and the angle θ at the apparent major axis. Using the Newton–Raphson method for nonlinear equations, we find $\epsilon = 0.07^{+0.08}_{-0.06}$ (99% CL) for UGC 4380, a solution *in*consistent with a circular disk. Derived values for the seven galaxies, plotted in Figure 4 and listed in Table 1, range from $\epsilon = 0.02$ to 0.20. Three galaxies (UGC 4380, NGC 2794, UGC 5274)

are inconsistent with having circular disks at the 99% CL; two galaxies (NGC 3890, NGC 5123) have ellipticities inconsistent with circular disks at the 95% CL. Only two galaxies (UGC 7208 and UGC 10436) are consistent with having circular disks within their 68% CL. The galaxies with the highest derived ellipticity ϵ have ϕ near 90°; the line of nodes is almost perpendicular to the true major axis. This is consistent with our selection of round, apparently face-on systems. The two galaxies with $\epsilon > 0.1$, NGC 2794 and UGC 5274, both show evidence for faint, interacting companions; NGC 2794 has an AGN.

Finally, we have checked that potential sources of systematic errors – lopsidedness, spiral structure, and warps – do *not* affect our ellipticity measurements appreciably. Table 1 contains the $\langle A_1 \rangle$ amplitude of the $m = 1$ component of the Fourier expansion of the light profile as defined by (Zaritsky & Rix, 1997). With the exception of NGC 5123 these galaxies are not significantly lopsided ($\langle A_1 \rangle < 0.2$), nor does $\langle A_1 \rangle$ correlate with our derived values for ψ or ϵ. None of these galaxies show any sign of kinematic asymmetry. A 180°-rotational asymmetry measure, defined as $A_{180} = |\sum(V_{obs} + V_{180})|/|2\sum V_{obs}|$, akin to the photometric asymmetry parameter of Conselice et al. (2000), yields close to null values for all.

Strong spiral structure drives photometric PAs to change with radius R at a rate of $\partial \mathrm{PA}/\partial \log R = \cot \theta_p$, where θ_p is the pitch angle of the arms. A warp in the disk also would be manifest as a twisting PA with radius. As discussed in §3, we make our photometric measurements between 3–4 scale-lengths where we find the photometric PA and axis ratio are constant, and our azimuthal variance statistic (Figure 1) corroborates that spiral structure is no longer a dominant photometric effect. The velocity fields exhibit no residual structure correlating with radius or azimuth, despite the fact that these measurements are *within* 3 scale-lengths (in contrast to our photometric measurements). We find no evidence for twisting PAs in the velocity fields which is not surprising since even galaxies with strong outer warps usually have planar HI distributions within 3 scale lengths (Briggs, 1990).

5. SUMMARY AND DISCUSSION

We have demonstrated that high-quality Hα velocity maps and I band images of nearly face–on galaxies can be used to *exclude the hypothesis that galaxy disks are intrinsically free of* $m = 2$ *(elliptic) distortions.* Our method for estimating the deviation from circularity suggests UGC 4380 has an intrinsic ellipticity of ∼7%. This is one of the first unambiguous detections of disk ellipticity for an individual galaxy. If disks are intrinsically elliptic, the photometric and kinematic axes will be misaligned in general, and the inclinations derived from isophote shapes will differ from the kinematic inclinations. Deviations are particularly large for face–on galaxies. WIYN/Densepak echelle spectroscopy and optical imaging are efficient means to estimate disk ellipticity for large samples of such systems.

The intrinsic ellipticity for our 7 galaxies is $\epsilon = 0.05 \pm 0.01$ (error weighted mean and uncertainty), inconsistent with purely circular disks. Most of our targets are normal, intermediate-type spirals, typical of those selected for TF surveys. According to the Franx & de Zeeuw (1992), $\epsilon = 0.05$ should produce ∼50% of the observed TF scatter in red and near-infrared bands. The cause of disk ellipticity is currently unclear, e.g., halo triaxiality or non-uniform matter accretion could be responsible. If larger samples show disk ellipticity at these levels, this implies variations in either disk mass fractions or mass-to-light ratio of today's spiral galaxies must contribute under 0.1-0.2 mag dispersion in the luminosity of galaxies at a given rotation speed. High resolution cosmological simulations (e.g. Steinmetz & Navarro, 1999; van den Bosch, 2000) indicate that variance in disk mass fraction should only induce scatter *along* the TF relation, because halo contraction is greater for larger disk masses. Assuming the remaining scatter in the observed TF relation is dominated by differences in spiral galaxy mass-to-light ratios, this modest variance places strong constraints on the formation histories of such systems.

We thank S. Barden at NOAO and D. Sawyer at WIYN for making Densepak happen. This research was supported by the UW-Madison Graduate School, and NSF grants AST-9618849 and AST-9970780 (MAB).

REFERENCES

Andersen, D. R., Bershady, M. A., Sparke, L., Gallagher, J., Wilcots, E., van Driel, W., & Ragaigne, D. 2001, *in preparation*

Baldwin, J. E., Lynden-Bell, D., & Sancisi, R. 1980, MNRAS, 193, 313

Barden, S. C., Sawyer, D. G., & Honeycutt, R. K. 1998, SPIE, 3355, 892

Binney, J. & De Vaucouleurs, G. 1981, MNRAS, 194, 679

Bosma, A. 1981, AJ, 86, 1825

Briggs, F.H. 1990, ApJ, 352, 15

Conselice, C. J., Bershady, M. A., & Jangren, A. 2000, ApJ, 529, 886

Courteau, S. & Rix, H. W. 1999, ApJ, 513, 561

Franx, M. & De Zeeuw, T. 1992, ApJ Letters, 392, L47

Grøsbol, P. J. 1985, A&A Supplement Series, 60, 261

Haynes, M. P., Magri, C., Giovanelli, R., & Starosta, B. M. 1988, AJ, 95, 607

Haynes, M. P., van Zee, L., Hogg, D. E., Roberts, M. S., & Maddalena, R. J. 1998, AJ, 115, 62

Huizinga, J. E. & van Albada, T. S. 1992, MNRAS, 254, 677

Kornreich, D. A., Haynes, M. P., & Lovelace, R. V. E. 1998, AJ, 116, 2154

Kornreich, D. A., Haynes, M. P., Lovelace, R. V. E., & van Zee, L. 2000, AJ, 120, 139

Lambas, D. G., Maddox, S. J., & Loveday, J. 1992, MNRAS, 258, 404

Paturel, G., *et al.* 1997, A&A Supplement Series, 124, 109

Richter, O. G. & Sancisi, R. 1994, A&A Letters, 290, L9

Rix, H. W. & Zaritsky, D. 1995, ApJ, 447, 82

Rudnick, G. & Rix, H. W. 1998, AJ, 116, 1163

Schoenmakers, R. H. M., Franx, M., & De Zeeuw, P. T. 1997, MNRAS, 292, 349

Schoenmakers, R. H. M. 1999, Ph.D. Thesis from Rijkuniversiteit Groningen, Netherlands

Steinmetz, M. & Navarro, J. F. 1999, ApJ, 513, 555

Swaters, R. A., Schoenmakers, R. H. M., Sancisi, R., & van Albada, T. S. 1999, MNRAS, 304, 330

Teuben, P. J., Sanders, R. H., Atherton, P. D. & van Albada, G. D. 1986, MNRAS, 221, 1

Tully, R. B. & Fisher, J. R. 1977, A&A, 54, 661

van den Bosch, F.C. 2000, ApJ, 530, 177

Willick, J. A. 1999, ApJ, 516, 47

Zaritsky, D. & Rix, H. W. 1997, ApJ, 477, 118

TABLE 1

ID	b/a	$\mathrm{PA}_{\mathrm{phot}}$ (deg)	i_{kin} (deg)	$\mathrm{PA}_{\mathrm{kin}}$ (deg)	ψ (deg)	ϕ (deg)	ϵ	ϵ confidence limits 68%	95%	99%	$\langle A_1 \rangle$
UGC 4380	0.90±0.02	43±4	16.1±2.3	33.5±1.8	10±9	15±15	0.07	$^{+0.04}_{-0.04}$	$^{+0.06}_{-0.06}$	$^{+0.08}_{-0.06}$	0.06±0.02
NGC 2794	0.85±0.04	408±3	20.5±1.4	327.9±0.9	80±3	83±4	0.20	$^{+0.07}_{-0.07}$	$^{+0.11}_{-0.11}$	$^{+0.13}_{-0.13}$	0.04±0.02
UGC 5274	0.94±0.02	78±7	32.2±3.8	9.5±1.4	69±7	84±5	0.20	$^{+0.07}_{-0.06}$	$^{+0.12}_{-0.10}$	$^{+0.14}_{-0.11}$	0.07±0.02
NGC 3890	0.96±0.02	264±16	23.5±1.8	225.6±1.4	38±16	73±13	0.08	$^{+0.05}_{-0.04}$	$^{+0.07}_{-0.07}$	$^{+0.08}_{-0.08}$	0.13±0.06
UGC 7208	0.94±0.01	325±9	23.8±2.3	330.4±1.2	-5.4±9	101±90	0.03	$^{+0.04}_{-0.03}$	$^{+0.06}_{-0.03}$	$^{+0.08}_{-0.03}$	0.12±0.05
NGC 5123	0.92±0.01	163±4	22.2±1.1	153.0±0.5	10±4	44±27	0.03	$^{+0.02}_{-0.02}$	$^{+0.04}_{-0.03}$	$^{+0.04}_{-0.03}$	0.25±0.10
UGC 10436	0.87±0.03	270±3	30.6±1.4	267.1±0.7	3±3	64±90	0.02	$^{+0.06}_{-0.02}$	$^{+0.09}_{-0.02}$	$^{+0.11}_{-0.02}$	0.09±0.05

FIG. 1.— The radial dependencies of photometric position angle (PA; top panel), ellipticity (1-b/a; middle panel) of UGC 4380's I-band isophotes. The bottom panel shows the azimuthal surface-brightness variance around each isophotal ellipse, normalized by the expected shot-noise (source noise, σ_s, and sky plus read-noise, σ_b). This normalized variance is large (> 1) where spiral structure contributes to the overall variance budget. We measure the PA and b/a between 29 and 39 arcseconds where both the PA and axis ratio remain constant, the azimuthal surface-brightness variance is consistent with shot noise, and the signal to noise per pixel is greater than one.

FIG. 2.— The Densepak Hα velocity field of UGC 4380 (left panel) and the residuals between the velocity field and a simple model (middle panel; see text). Both are smoothed and interpolated using a polynomial surface. Solid, heavy, and dashed lines are positive, zero, and negative velocities, respectively, relative to the model systemic velocity (left panel) or model velocity field (middle panel). The dash-dotted lines (left panel) represent the isophotal annulus determined from Figure 1 from which the photometric b/a and PA are derived (solid lines in annulus indicate photometric major and minor axes). The right, summary panel shows a schematic diagram of an isophote for UGC 4380 assuming its disk has an intrinsic ellipticity of $\epsilon = 0.07$. The x-y plane has been rotated 33.5° from North to match the kinematic position angle of UGC 4380. The solid ellipse represents the true shape of the disk seen face-on; the major axis lies at an angle $\phi = 15°$ from the line of nodes (the kinematic major, or y axis). The dashed ellipse represents the apparent shape after inclining the elliptic disk by $i = 16.1°$; it has an apparent axis ratio of $b/a = 0.90$. The kinematic and photometric PAs differ by $\psi = 9.5°$.

FIG. 3.— Solutions for ellipticity ϵ and angle ϕ for seven sample galaxies. The 68% confidence limits (CL), shown as contours, are derived from the estimated measurement errors on b/a, ψ and i listed in Table 1. UGC 7208 (dark-dash) and UGC 10436 (light dash) are consistent with a circular disk within the 68% CL.

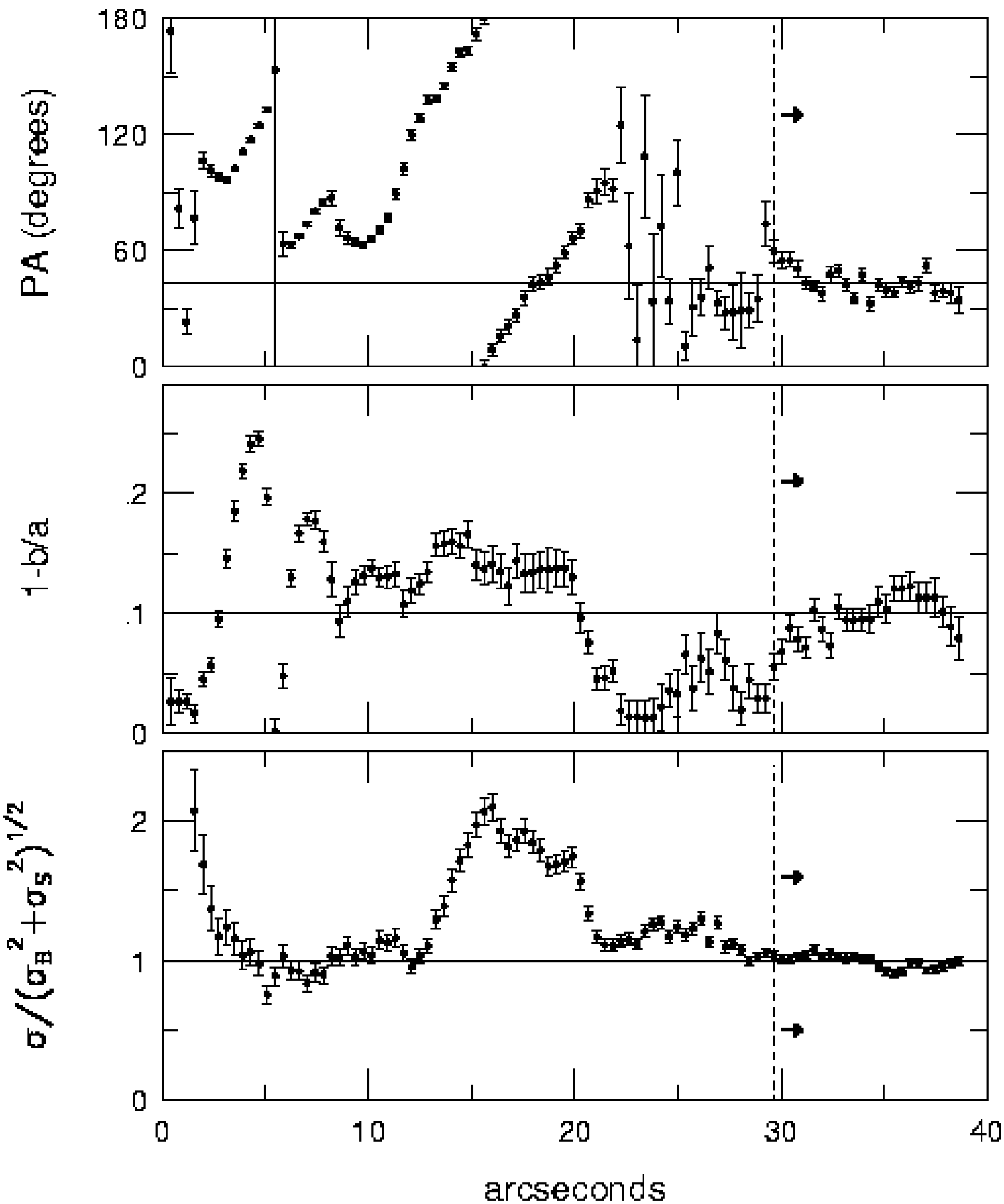

PA (degrees)
180
120
60
0
1-b/a
.2
.1
0
$\sigma/(\sigma_B^2+\sigma_S^2)^{1/2}$
2
1
0
0
10
20
30
40
arcseconds

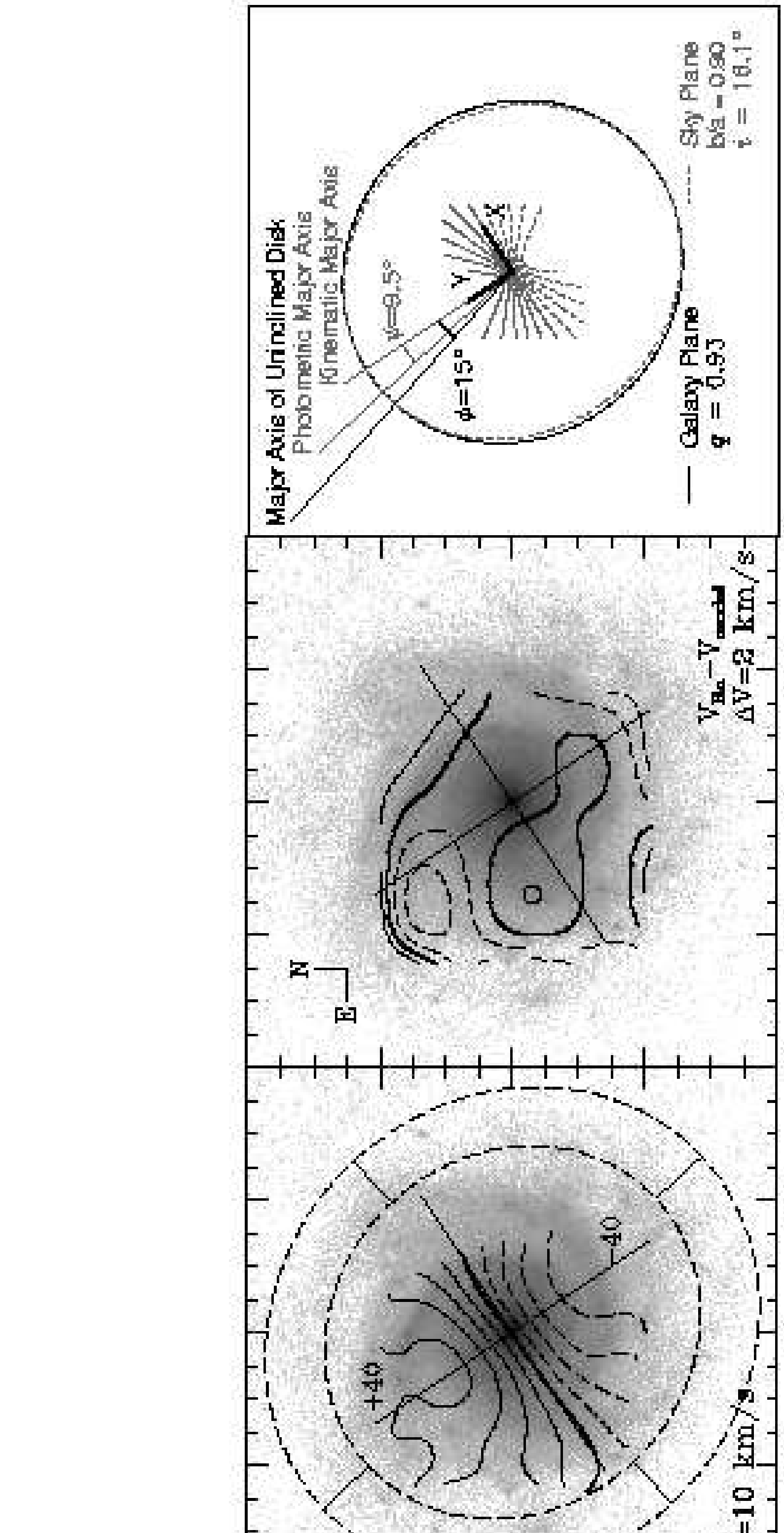
arcseconds
+40
-40
N
E
Major Axis of Uninclined Disk
Photometric Major Axis
Kinematic Major Axis
ψ=9.5°
φ=15°
X
Y
Galaxy Plane
q = 0.93
Sky Plane
b/a = 0.90
i = 16.1°

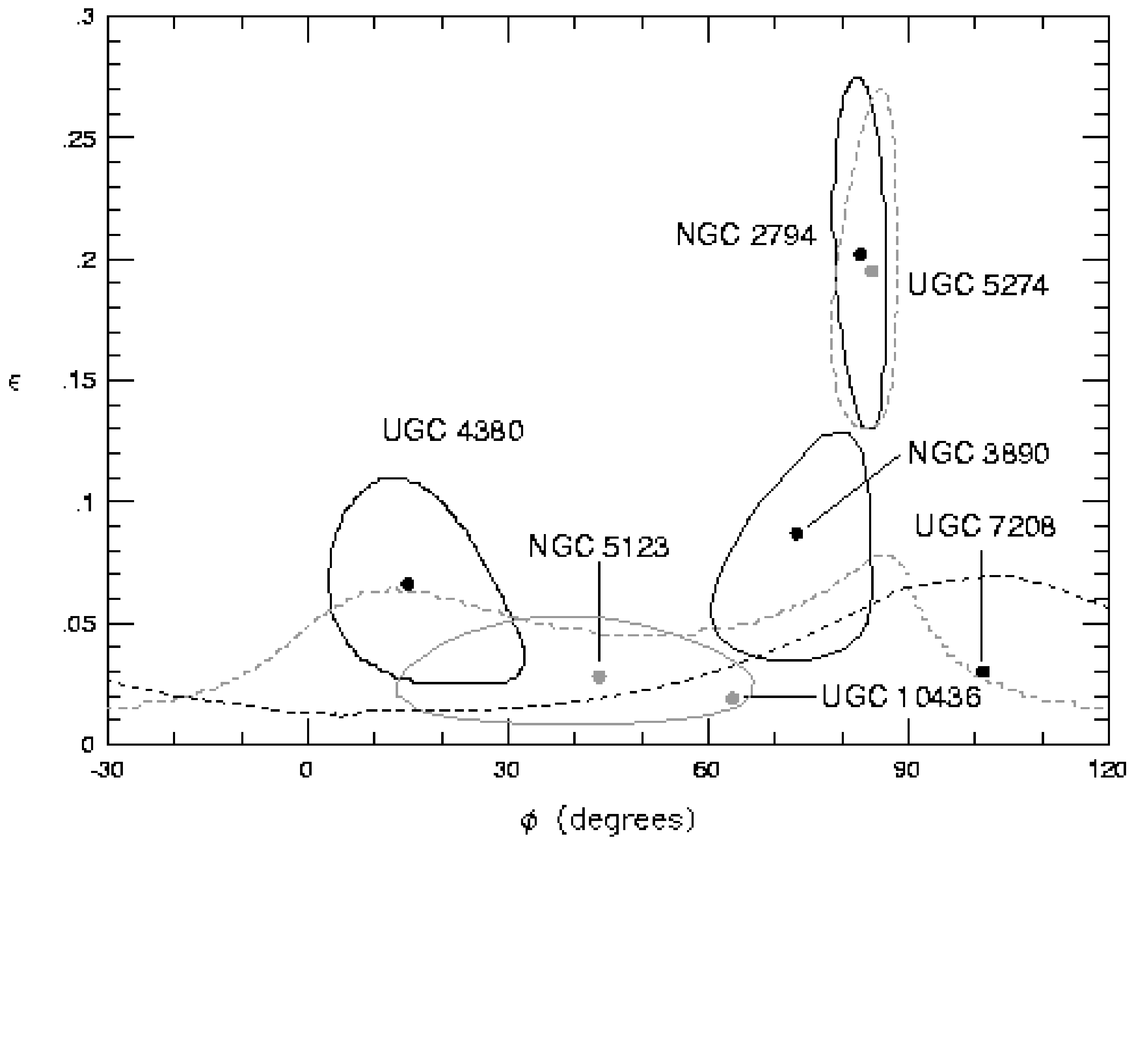

.3
.25
.2
.15
.1
.05
0
ε
-30
0
30
60
90
120
φ (degrees)
NGC 2794
UGC 5274
UGC 4380
NGC 3890
UGC 7208
NGC 5123
UGC 10436